To appear in the *SREW Proceedings*, 2000.

Energy and spatial dependence of the east-west effect observed by Mir-REM

Paul Bühler, Alex Zehnder,

Paul Scherrer Institute, Laboratory for Astrophysics, 5232 Villigen, PSI, Switzerland

Michel Kruglanski

Belgian Institute for Space Aeronomy, 1180 Brussels, Belgium

Eamonn Daly

ESTEC, NL-2200 AG Noordwijk, The Netherlands

Abstract

In the South Atlantic Anomaly the energetic proton fluxes are anisotropic. Fluxes from west are higher than those from east. Using data from the Radiation Environment Monitor aboard the Russian orbital station Mir, we determined the energy and spatial dependence of the west-east proton flux ratio. We find the energy spectra of the east-fluxes to be softer than those from west, and the effect to be a decreasing function of the L-shell parameter, and vanishes above $L \approx 1.7\ R_E$. Comparison with model calculations show that existing models used to describe the anisotropy can not reproduce the observed spatial variations in a consistent way.

Introduction

The LEO orbits are the preferred orbits for manned space missions, like Mir, Space Shuttle, ISS. In such an orbit an important contribution to the total radiation dose occurs in the South Atlantic Anomaly, SAA [*Konradi et al.,* 1994; *Badhwar et al.,* 1996; *Bühler et al.,* 1996] and is caused by the high energetic trapped protons of the inner radiation belt. It is therefore of vital interest to have accurate models of this particle population.

A special feature of the SAA is the anisotropy of the proton fluxes. The anisotropy is caused by the fact, that at a given position trapped particles arriving from different directions have their guiding centers at different locations and therefore belong to different drift-shells. This is true anywhere in the magnetosphere. But if the difference in guiding center position is large compared to the scale length of the spatial flux gradient then the locally observed flux distribution can be expected to be anisotropic [*Lenchek and Singer,* 1962].

At low altitudes the trapped proton population is controlled by the Earth's atmospheric density and its altitude gradient, which leads to strong flux gradients in the SAA. The difference in guiding center location for particles arriving from opposite directions scales with the gyro-radius. The gyro-radius depends on the particle's momentum p, and on the magnetic field strength, B with $r_{gyro} = p/(q \cdot B)$. The anisotropy is therefore best observed with high momentum particles at low magnetic fields. The Russian orbital station Mir encounters the minimum field strength of approximately 0.2 $Gauss$ in the SAA. There the gyro-radius of 100 MeV protons is of the order of 100 km and comparable in size with the scale length of the flux gradients. It is therefore the proton fluxes in the SAA for which the anisotropy can be best observed.

The effect is a function of energy and can also be expected to depend on the local magnetic field configuration, thus to be a function of magnetic coordinates B and L-shell parameter, L. It has been measured at selected locations and energies [*Heckman and Nakano,* 1969; *Konradi et al.,* 1994; *Looper et al.,* 1998; *Bühler et al.,* 1998; *Sakaguchi et al.,* 1999] and has been shown to be important.

In this paper we investigate the spatial and energy dependence of the difference in proton fluxes arriving from magnetic east and west, in the SAA.

Observations and data analysis

Observations

For this analysis we used proton data from the Radiation Environment Monitor, REM aboard Mir [*Bühler et al.,* 1996]. REM was mounted outside the Mir space station and was working from November 1994 to November 1996. REM consists of two independent shielded silicon detectors and measures the energy deposit of charged particles. The silicon diodes are 300 μm thick and have an active area of 150 and 25 mm^2. Data of each detector was accumulated and binned into 16 energy deposit bins, covering the range from 100 keV to over 100 MeV, with a temporal resolution of 32 seconds. The shielding of the detectors consist of a thick aluminum cone and spherical shields of aluminum and tantalum of > 0.19 g/cm^2 for one of the detectors and > 2.06 g/cm^2 for the other detector. The lower proton energy threshold is therefore around 10 MeV. Whereas the heavier shield of one detector efficiently stops electrons of several MeV, the lower energy threshold for electrons of the less shielded detector is around 1 MeV.

The aluminum cone restricts the direct field of view of the detectors to $\pm 45°$. REM was mounted at the outside of Mir looking into free space and was therefore very well shielded from the backside by the space station.

Mir is in a practically circular Low Earth Orbit, LEO, at an altitude of ≈ 400 km, an inclination of 52°, and a period of 90 minutes. It scans several times per day through the SAA region, with varying orientation.

Data mapping

For each Mir-REM data point we determined the satellite position $\vec{s}$ and the look direction of REM, $\vec{o}_{REM}$, for which the necessary information was provided by the Mir control center ENERGIA, and computed the local magnetic field vector, $\vec{B}$, and L-shell parameter, L for locally mirroring particles with the IGRF 95 magnetic field model.

We then selected data points in the inner radiation belt ($1.1 < L < 2.6$) for which the cosine of the angle between $\vec{o}_{REM}$ and magnetic east or west was larger than 0.81, where magnetic east and west are defined by $-\vec{s} \wedge \vec{B}$ and $\vec{s} \wedge \vec{B}$, respectively. The two groups of data, east and west, were then binned into B-L-bins of 0.05 R_E and 0.001 $Gauss$. The histograms in each bin were finally averaged over the entire mission.

In such a way we obtained temporally averaged B-L-maps of REM histograms for east and west looking REM orientations.

Figure 1

Figure 1 shows an extract of the such determined maps at $1.3 < L < 1.35\ R_E$. In the large panel the count rates in counts/sec of the heavier shielded detector (sum of detector channels 4 and 5 (240 $< E_{dep} <$ 360 keV) representing $> 200\ MeV$ protons) is plotted versus B. The asterisks show the data with REM looking in magnetic west direction, and the diamonds the data with REM looking in magnetic east direction. The dashed lines show the background corrected count rates. Over a large range of B-values, which covers a flux range of more than two orders of magnitude, the west-rates are significantly higher than the east-rates. At large B-values the two curves merge and flatten out. There the proton fluxes are very low and the REM count rates are dominated by electrons and cosmics. This part is used to determine the background.

The four small panels show the relative count rate histograms of the heavier shielded detector in selected B-bins. The upper two panels show histograms at $0.199 < B < 0.200\ Gauss$ (left) and $0.211 < B < 0.212\ Gauss$ (right) with REM looking west. The lower two panels show histograms in the same B-bins but with REM looking east. The shapes of the histograms allow to qualitatively judge the energy spectrum of the incident particles. Compared with the west-histograms, the east-histograms are biased towards the higher channels, indicating the east spectra to be softer than the west spectra. This indeed can be expected since the high energy particles coming from east are members of drift shells dipping on average deepest into the atmosphere which explains why the east fluxes are low and their spectra soft.

Compared to the difference observed in east-west direction, the histograms at different B are very similar, indicating the proton spectra in a given L-bin only to change little as function of the magnetic field.

Spectral information

The REM histograms can be used to deduce the incident particle energy spectra. The count rate in detector channel i, cr_i in units of $1/sec$ is related to the incident differential particle spectra $f_k(E)$, where index k indicates the particle species, by

$$cr_i = \sum_k \int_0^\infty f_k(E) \cdot G_k(i, E) dE \qquad (1)$$

$f_k(E)$ is given in units of $1/sec/cm^2/MeV$ and $G_k(i,E)$ is the energy, detector channel, and particle species dependent geometric factor and is given in units of cm^2. The geometric factors were determined by calibrations in a proton beam and betatron, and with numerical simulations including a model for the mass distribution of the space station [*Ljungfelt,* 1993; *Hajdas et al.,* 1993]. For the analysis of the REM data in the SAA we assume only protons and electrons to be relevant and neglect any other contribution to the detections.

In order to invert equation (1) the proton and electron spectra are parameterized. We approximated the shape of the proton energy spectra by a power law, $f_p(E) = f_p(E_{p0}) \cdot (E/E_{p0})^{\gamma_p}$ with $E_{p0} = 30\ MeV$ and the shape of the electron spectra by an exponential function, $f_e(E) = f_e(E_{e0}) \cdot exp(-\gamma_e \cdot (E - E_{e0}))$ with $E_{e0} = 1.0\ MeV$. The normalizations and spectral indices are free parameters and are simultaneously determined by a numerical fit of the measured detector count rates with equation (1). The method yields good proton spectral characterization only in B-L-bins where the proton fluxes contribute a non-neglectable number of counts to the count rates. This is the case at $1.1 < L < 2.2\ R_E$ and the low B-values.

The left panel of figure 2 shows a grey-scale B-L-map of the 100 MeV proton flux west-east ratio. Note, that the white area below the grey shaded area is not sampled by Mir, and that in the white area above, the proton contribution is too small to allow the determination of proton spectral parameters with REM. The right panel shows analogously the west-east ratio of the proton spectral indices. figure 2

The east-west effect is clearly a function of L. The flux ratio is largest at small L, continuously decreases with increasing L, and becomes 1 above $L \approx 1.7\ R_E$. The same behavior is also found for the spectral index. Below $L \approx 1.7\ R_E$ the east spectra are softer than the west spectra, as indicated by the histograms shown in figure 1, but the difference decreases with increasing L. For a given L-bin there is no obvious magnetic field dependence.

Comparison with models

In the following we compare the REM measurements with two models of the east-west effect and especially address the question whether the models are able to describe the observed L-dependence.

Local model

Lenchek and Singer, 1962 argued that the flux gradients in the SAA are mainly caused by the interaction of the particles with the upper atmosphere and that the proton fluxes in first approximation could be directly related to the gyration averaged atmospheric density. But since the atmospheric density is a function of altitude, the proton fluxes could be expressed as function of altitude of their guiding centers.

The difference in altitude of the guiding center and the point of observation, dh is given by

$$dh = r_{gyro}(E) cos(I) sin(\beta) \tag{2}$$

where I is the dip angle of the local magnetic field line, and β is the azimuthal angle, with $\beta = -90°$ is east and $\beta = +90°$ is west.

In the following it is assumed, as done by *Lenchek and Singer* [1962], that the proton fluxes are inversely proportional to the atmospheric density, ρ_{atm} at the guiding center location. Then using different approaches for the altitude dependence of the atmospheric density and equation (2), the west-east flux ratio can be calculated. In table 1 two cases are listed. Both models have a free parameter, which can be computed by applying the formulas in the last column of table 1 to the data.

table 1

We have done that for the B-L-bins with the lowest B-values at a given L. The results are presented in figure 3 as function of L. The two uppermost panels contain the proton flux normalization at 30 MeV and the spectral power law indices, respectively. The dotted lines are smoothed curves through the data points. The following panels show the proton flux ratio, the cosine of the averaged magnetic field dip angle in the given B-L-bin, H_0, and n at 50 MeV (bold line) and 200 MeV (dotted line), respectively. The vertical errorbars represent the statistical errors. The curves without dots in panels 3, 5, ad 6 show the results computed with the smoothed curves of the two uppermost panels.

figure 3

The resulting atmospheric scale height H_0 increases continuously from around 100 km at $L = 1.1\ R_E$ to about 300 km at $L = 1.6\ R_E$ but then starts to attain unreasonable values. This is a consequence of the formula for H_0 given in table 1. When the flux ratio f_{west}/f_{east} approaches the value 1, the denominator becomes very small, and thus H_0 grows infinitively. At lower L-values the H_0 value compares not too badly with the ≈ 60 km found by *Heckman and Nakano* [1963]. However, if H_0 is thought to be a characteristic quantity of the atmosphere it should not depend on L. The same is true for the altitude power law index n. However, n has no singularity and is a smooth function of L. *Heckman and Nakano* [1969] found n to be around 4 to 5, which is somewhat higher than our results. We must remind here that REM has a rather large acceptance angle such that therefore the 'true' east-west ratio can be expected to be higher than the values we measure with REM. So the 'true' H_0 can be expected to be somewhat smaller and the 'true' n, larger than our results.

If we assume H_0 and n to be independent of L, the L-dependence of the east-west effect in these local models is given by the L-dependence of dh, which, according to equation (2) is defined by the L-dependence of the magnetic dip angle I. In this case the east-west ratio can reach the value 1 only where $I = 90°$, which however is nowhere the case (see panel 4 of figure 3) in the investigated region.

It must be noted that an L-dependence of H_0 and n can be introduced by considering these parameters to reflect the interaction of the protons with the atmosphere. In this case, since this interaction takes place everywhere along the particle trajectories, these 'effective' parameters could be assumed to be functions of the drift shell (i.e. B and L) [*Heckman and Brady,* 1969]. However, since the interaction is strongest at the lowest mirror points on a given drift shell, which for the here investigated cases are all located in the SAA, little variations of the 'effective' H_0 and n can be expected over the investigated L-range.

Generalized model

Kruglanski et al. [1998, 1999] assumed that the directional proton flux at a given location, $f(E, \alpha, \beta)$ is the perpendicular flux at the guiding center location and can be written as

$$f(E, \alpha, \beta) = f_\perp(E, B_{GC}, L_{GC}) \tag{3}$$

where B_{GC} and L_{GC} are the magnetic field strength and L-value at the guiding center location of the particles. α is the pitch angle and β the azimuthal angle. In order to avoid the calculation of B_{GC} and L_{GC} they expanded the expression in equation (3) to first order in L and in addition made the approximation $B_{GC} = B$. The derived expression for the directional proton flux is

$$f(E, \alpha, \beta) \approx f_\perp(E, B, L) + \Delta L \cdot \left.\frac{\partial f_\perp}{\partial L}\right|_{E,B} \tag{4}$$

where $\Delta L = L_{GC} - L$. They further derived an analytical expression for ΔL which only depends on local quantities such that the directional proton flux can be expressed as

$$f(E,\alpha,\beta) \approx f_\perp(E,B,L) + \left(\frac{E^2 + 2m_0c^2E}{qc\sqrt{MBL^{-3}}}\right) sin\beta \cdot \left.\frac{\partial f_\perp}{\partial L}\right|_{E,B} \quad (5)$$

with m_0 the proton rest mass, q the proton charge, and M the earth's magnetic dipole moment.

With this approximation the west-east flux ratio for locally mirroring particles can be expressed as

$$f_{west}/f_{east} = \frac{f(E,90°,90°)}{f(E,90°,-90°)} \quad (6)$$

Besides some fundamental constants this relation contains only local quantities, the perpendicular flux $f_\perp(E,B,L)$ and its derivative $\left.\frac{\partial f_\perp}{\partial L}\right|_{E,B}$.

figure 4

Equation (6) can be solved for $\frac{\partial f_\perp}{\partial L}$ and using the measured west-east flux ratios and $f_\perp(E,B,L) = (f_{west} + f_{east})/2$, $\frac{\partial f_\perp}{\partial L}$ is determined. The result of this computation is shown in figure 4. Like in figure 3, we show the results for the B-L-bins with the lowest B value at a given L and plot them as function of L. The upper most panel shows our estimate of $f_\perp$ and the middle panel shows $\left.\frac{\partial f_\perp}{\partial L}\right|_{E,B}$, computed with equation (6). Bold and dotted lines show results at 50 and 200 MeV and the vertical errorbars represent the statistical errors.In order to compare these values with the 'true' derivations, we computed $\left.\frac{\partial f_\perp}{\partial L}\right|_{E,B}$ with the AP8 flux model. For each B-L-bin we extracted from AP8 the $f_\perp(L)$-curve at the corresponding B-value and computed the derivation with respect to L. The such computed values are shown in the lower most panel of figure 3. Squares and diamonds show the computed values at 50 and 200 MeV, and the bold and dotted lines are corresponding polynomial fits which are added to guide the eye.

There are significant differences between the two sets of curves, in amplitude and shape. Whereas the derivations computed from equation 6 are positive over the investigated range and vanish, according to equation 6, where the west-east ratio becomes 1 (around $L = 1.7\ R_E$), the AP8-curves cross the 0-line between 1.4 and 1.5 R_E and become negative at higher L-values. The AP8 model suggests that above $L \approx 1.5\ R_E$ the slopes of the $f_\perp(L)$-curves are negative. According to equation 6 the west-east ratio would have to become smaller than 1 in this region, which is not observed.

The Kruglanski model takes the flux gradients along L into account but neglects the gradients along B. This approximation is only valid as long as $dB = B_{GC,west} - B_{GC,east}$ is smaller than the scale length of the flux gradients along B. Assuming, that the east and west guiding centers are separated by a gyrodiameter we find that for 200 MeV protons dB is a function of L and decreases from around 0.02 $Gauss$ at $L = 1.1\ R_E$ to approximately 0.005 $Gauss$ at $L = 2\ R_E$. Figure 1 shows that these dB-values are important compared to the scale length of the flux gradients along B. The neglection of a dB term in equation (4) may therefore not be justified in the relevant B-L-area. These estimates show further that dB is a decreasing function of L and therefore shows the same trend as the west-east ratio. dL in contrary increases with L, from around 0.2 R_E at $L = 1.1\ R_E$ to below 0.1 R_E at $L = 2\ R_E$ This might indicate, that the dB-term may even be dominating. Introduction of a ΔB-term in equation 4 could improve the results.

It is interesting to note, that dB and dL in a given L-bin are practically independent of B and therefore the east-west effect, in first approximation can be expected not to depend on B, which is in agreement with our measurements (see figure 2).

Summary and conclusions

When comparing the presented measurements with model calculations and other observations it must be kept in mind that the presented measurements have been made with a wide-angle instrument. As a consequence the measured west-east ratios represent a lower limit for the true values. This affects the absolute values but not the qualitative characteristics, like the energy and L-dependence, which we emphasize in this paper.

The measurements show, that

- over a wide L and B range the proton fluxes arriving from west are higher than the particle fluxes coming from east
- the east-spectra are softer than the west-spectra
- the west-east ratio is a decreasing function of L and becomes 1 above $L \approx 1.7\ R_E$

Non of the models tested here can describe the observed L-dependence in a consistent way. The model parameters H_0, n, and $\left.\frac{\partial f_\perp}{\partial L}\right|_{E,B}$ as function of L do not behave as expected. The models use approximations which, although giving good results at selected locations, may not be valid over a larger area.

Nevertheless, if the model parameters are considered to be free parameters which depend on B, L and E, then the models together with the determined parameter values can be at least used to describe the expected west-east ratio in a relatively simple way.

With the start of operation of the International Space Station increased attention is payed to the prediction of the radiation environment in the SAA. Tools are needed which allow to calculate the particle flux distributions in an effective way. The presented results may be used as a guideline for the development of such improved models.

Acknowledgments. This work was supported by ESA's Technology Research Program, ESA/TOS-EMA, Space Environments and Effects Major Axis.

References

Badhwar, G.D., Atwell, W., Cash, B., Petrov, V.M., Akatov, Y.A., Tchernykh, I.V., Shurshakov, V.A., and Arkhangelsky, V.A., Radiation environment on the Mir orbital station during solar minimum, *Adv. Space Res., 22,* 501, 1998.

Bühler, P., Desorgher, L., Zehnder, A., Daly, E., Adams, L., Observations of the low earth orbit radiation environmnet from Mir, *Rad. Measurements, 26,* 917, 1996.

Bühler, P., Ljungfelt, S., Mchedlishvili, A., Schlumpf, N., Zehnder, A., Adams, L., Daly, E., Nickson, R., Radiation environment monitor, *Nucl. Instr. and Meth. in Phys. Res. A, 368,* 825, 1996.

Bühler, P., Desorgher, L., Zehnder, A., Daly, E., Adams, L., REM measurements aboard Mir during 1995, *Adv. Space Res., 21,* 1645, 1998.

Hajdas, W., Ljungfelt, S., and Cordt, I., Test of the REM detector on the betatron, *Ann. Report, IIIA,,* 155 pp., Paul Scherrer Institute, 5232 Villigen PSI, Switzerland, 1993

Heckman, H.H. and Nakano, G.H., East-west asymmetry in the flux of mirroring geomagnetically trapped protons, *J. Geophys. Res., 68,* 2117, 1963

Heckman, H.H. and Brady, V.O.., Effective atmospheric losses for 125-MeV protons in the south atlantic anomaly, *J. Geophys. Res., 71,* 2791, 1966

Heckman, H.H. and Nakano, G.H., Low-altitude trapped protons during solar minimum period, *J. Geophys. Res., 74,* 3575, 1969

Konradi, A., Badhwar, G.D., and Braby, L.A., Recent space shuttle observations of the south atlantic anomaly and the radiation belt models, *Adv. Space Res., 14,* 911, 1994

Kruglanski, M., Heynderickx, D., and Lemaire, J., Proton Anisotropy, *TREND-3 final report, Radiation environments of astronomy missions and LEO missions,* 35 pp., BIRA-IASB, Belgium,1998

Kruglanski, M. and Heynderickx, D., Analysis of the low-altitude proton flux asymmetry: methodology, *Rad. Meas., 30,* 645, 1999

Lenchek, A.M. and Singer, S.F., Effects of the finite gyroradii of geomagnetically trapped protons, *J. Geophys. Res., 67,* 4073, 1962

Ljungfelt, S., Calibration of the Radiation Environment Monitor, *Ann. Report, IIIA,,* 153 pp., Paul Scherrer Institute, 5232 Villigen PSI, Switzerland, 1993

Looper, M.D., Blake, J.B., Mewaldt, R.A., Maps of hydrogen isotopes at low altitudes in the inner zone from SAMPEX observations, *Adv. Space Res., 21,* 1679, 1998

Sakaguchi, T., Doke, T., Hasebe, B., Kikuchi, J., Kono, S., Takagi, T., Takahashi, K., Nagaoka, S., Nakano, T., Takahashi, S., and Badhwar, G., Measurement of the directional distribution of incident particles in the Shuttle-Mir mission orbit, *J. Geophys. Res., 104,* 22793, 1999

P. Bühler, A. Zehnder., Laboratory for Astrophysics, Paul Scherrer Institute, 5232 Villigen, PSI, Switzerland (e-mail: paul.buehler@psi.ch; alex.zehnder@psi.ch)

M. Kruglanski, Belgian Institute for Space Aeronomy, 1180 Brussels, Belgium (e-mail: michelk@mail.magnet.oma.be)

E. Daly, ESTEC, NL-2200 AG Noordwijk, The Netherlands (e-mail: eamonn@wm.estec.esa.nl)

This preprint was prepared with AGU's LATEX macros v5.01. File ew˙paper˙1 formatted November 8, 2000.

Figure 1. REM count rates in counts/sec, representing $> 200\ MeV$ protons, versus B at $1.3 < L < 1.35\ R_E$ for west (asterisks) and east (diamonds) looking detector. The small panels show energy deposit histograms in the heavier shielded REM detector at two different B-values for west (upper panel) and east (lower panel) oriented detector. The bias to higher detector channels in the east-histograms indicates a soft incident proton spectrum. Note, that the histograms change only little as function of the magnetic field.

Figure 2. Grey-scale maps of the (left panel) 100 MeV proton flux west-east ratio and (right panel) spectral powerlaw west-east ratio. The ratios are decreasing functions of L and become 1 above $L \approx 1.7\ R_E$.

Figure 3. Local model parameters as function of L. The two uppermost panels show the proton spectral normalisation at 30 MeV and the power law spectral indices for west (asterisks) and east (diamonds) looking detector. The following panels show the west-east ratio, cosine of local magnetic field line dip angle, atmospheric scale height H_0, and altitude power law index n at different energies. The curves show the values of the B-L-bins with the lowest B-value encountered by Mir at a given L.

Figure 4. Generalized model parameters as function of L. The panels show (t.t.b.) the perpendicular proton flux $f_\perp$ and the the generalized model parameter $\left.\frac{\partial f_p}{\partial L}\right|_{B,E}$ as computed with equation 6 and with the AP8 model.

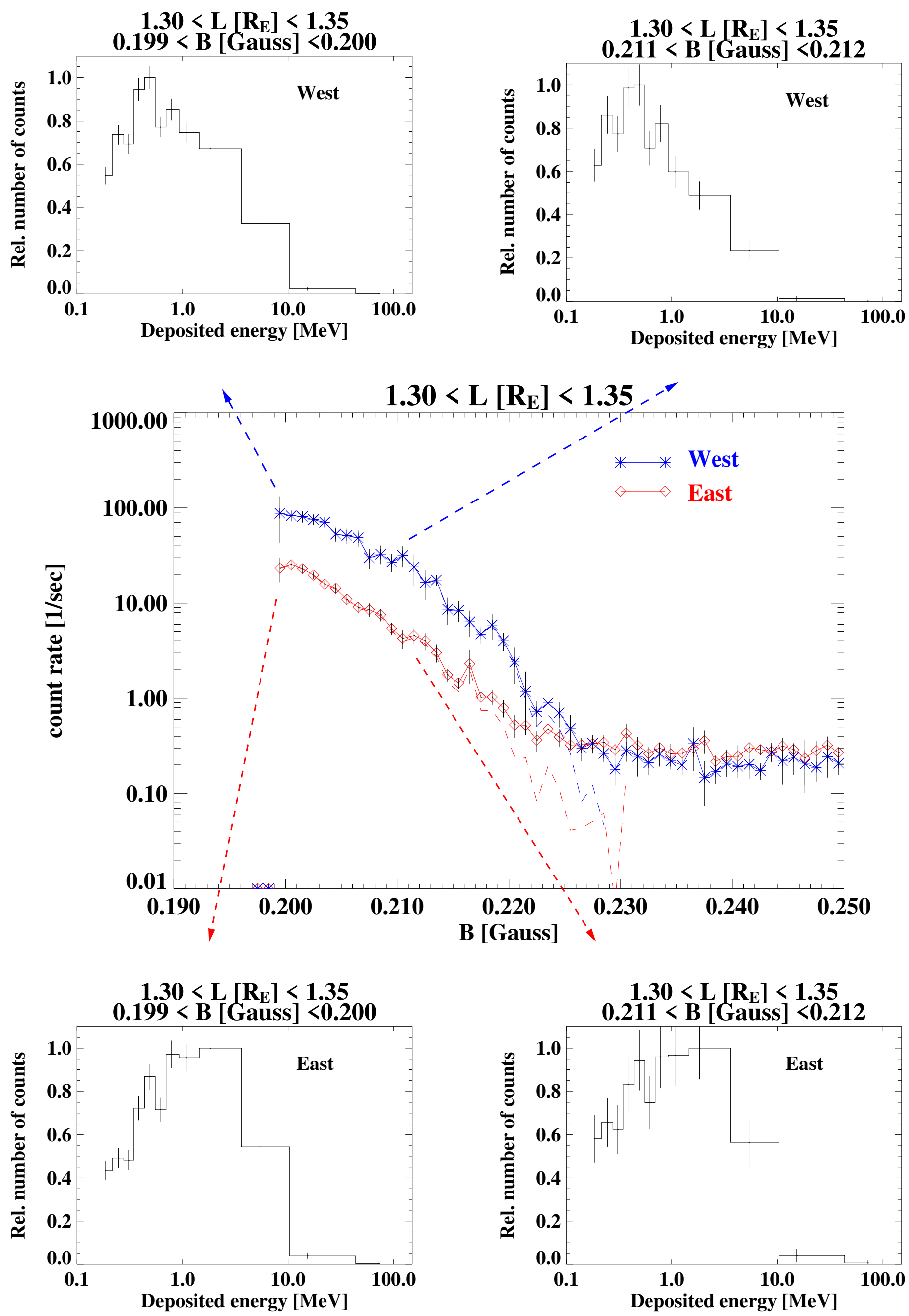
1.30 < L [R$_E$] < 1.35
0.199 < B [Gauss] <0.200
West
Rel. number of counts
Deposited energy [MeV]
1.30 < L [R$_E$] < 1.35
0.211 < B [Gauss] <0.212
West
1.30 < L [R$_E$] < 1.35
West
East
count rate [1/sec]
B [Gauss]
1.30 < L [R$_E$] < 1.35
0.199 < B [Gauss] <0.200
East
1.30 < L [R$_E$] < 1.35
0.211 < B [Gauss] <0.212
East

Figure 1.

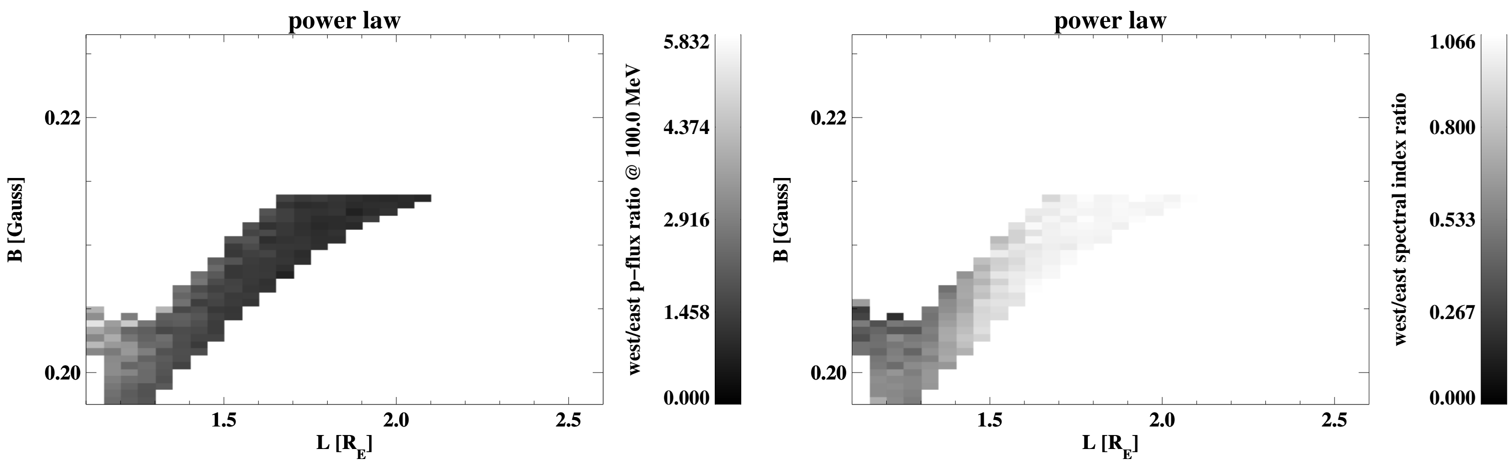

power law
B [Gauss]
0.22
0.20
1.5
2.0
2.5
L [R$_E$]
west/east p−flux ratio @ 100.0 MeV
5.832
4.374
2.916
1.458
0.000
power law
B [Gauss]
0.22
0.20
1.5
2.0
2.5
L [R$_E$]
west/east spectral index ratio
1.066
0.800
0.533
0.267
0.000

Figure 2.

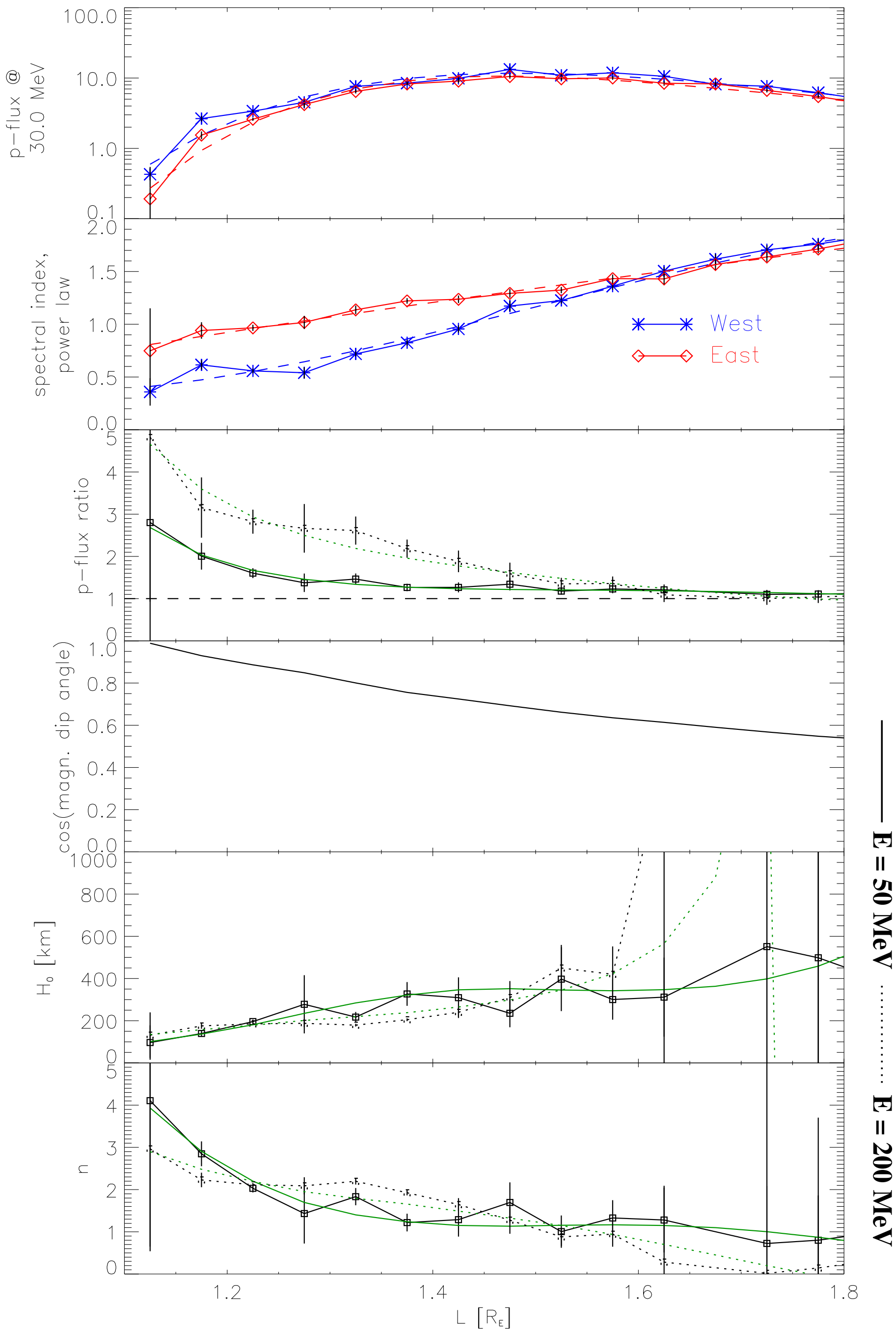

p−flux @ 30.0 MeV
spectral index, power law
West
East
p−flux ratio
cos(magn. dip angle)
H₀ [km]
n
L [R_E]
E = 50 MeV
E = 200 MeV

Figure 3.

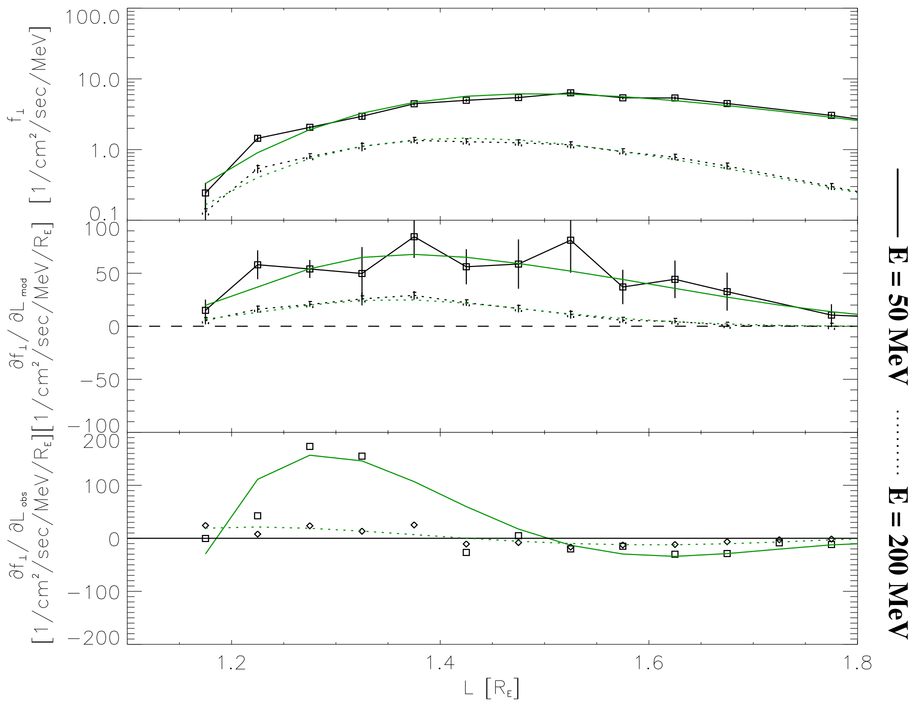

E = 50 MeV
E = 200 MeV
$f_\perp$ [1/cm²/sec/MeV]
$\partial f_\perp / \partial L_{mod}$ [1/cm²/sec/MeV/R$_E$]
$\partial f_\perp / \partial L_{obs}$ [1/cm²/sec/MeV/R$_E$]
L [R$_E$]

Figure 4.

Table 1. Atmospheric density - altitude relations and resulting west-east proton flux ratios.

Atmospheric density model $\rho_{atm} \propto$	west-east ratio $f_{west}/f_{east} =$	free parameter
$^{(1)} exp(-h/H_0)$	$exp(dh/H_0)$	$H_0 = dh/ln(f_{west}/f_{east})$
$^{(2)} h_0^{-n}$	$\left(\frac{h_0+dh/2}{h_0-dh/2}\right)^n$	$n = \frac{ln(f_{west}/f_{east})}{ln\left(\frac{h_0+dh/2}{h_0-dh/2}\right)}$

(1) [*Lenchek and Singer*, 1962]
(2) [*Heckman and Nakano*, 1969]